

# RXTE/OSSE Fits to the Hard State Spectrum of Cygnus X-1

Thomas J. Maccarone

*Scuola Internazionale Superiore di Studi Avanzati, via Beirut, n. 2-4, Trieste, Italy, 34014*

Paolo S. Coppi

*Department of Astronomy, Yale University, P.O. Box 208101, New Haven CT USA 06520-8101*

## ABSTRACT

We present three spectra of Cygnus X-1 in the low/hard state from 3-1000 keV produced with RXTE and OSSE. We demonstrate that a pure thermal Comptonization model, with Compton reflection fits the data well, with coronal temperatures of about 90 keV, optical depths of about 1.3, and reflection fractions of about  $0.25 \times 2\pi$ . We find that no additional components are necessary to fit the data, although the presence of an additional non-thermal component does result in a marginal improvement to the goodness of the fit. Two of the observations are fit better by an almost purely non-thermal Comptonization model with  $\Gamma_{inj}$  of  $\sim 3.2$  for the electrons and the other parameters essentially the same as for the thermal model, while the third observation is also consistent with this model. Observations that could break this degeneracy are discussed. We also demonstrate that the low reflection parameter (i.e.  $R/2\pi < 1$ ) is due to a lack of strong curvature in the 30-50 keV range of the spectrum and not due to ionization effects. The spectrum changes very little over the three weeks of the observations, in accordance with a three week correlation timescale found in the All Sky Monitor data. We show that for a purely thermal corona, the radius of the corona must be between  $3 \times 10^6$  and  $1.5 \times 10^{10}$  cm, while the radius of a hybrid corona or a purely non-thermal corona is constrained to be between  $10^8$  and  $10^9$  cm.

**Key words:** accretion, accretion disks – X-rays:binaries – X-rays:individual: Cygnus X-1

## 1 INTRODUCTION

Cygnus X-1 is a binary star system consisting of an O9.7 Iab supergiant (Gies & Bolton 1986) and a compact object of at least 6 solar masses (Dolan 1992). The compact object accretes matter from a focused wind off the supergiant star (Gies & Bolton 1986) and is one of the brightest persistent sources of X-rays in the sky. Cyg X-1 is the first system to show strong evidence of containing a black hole and remains one of the strongest candidates for being a black hole.

Phenomenologically, the spectrum of Cygnus X-1 above  $\sim 3$  keV is well described as an exponentially cutoff power law with a photon spectral index of  $\Gamma \sim 0.6-0.7$  and a cutoff energy of around 150 keV. Additionally the spectrum shows a broad excess around 30-50 keV due to Compton reflection, an iron K edge above 7 keV and an iron  $K\alpha$  fluorescence emission line (see e.g., Ebisawa 1996). The hard power law has generally been described as arising from thermal Comptonization of soft photons in a hot, photon starved corona

(Sunyaev & Trümper 1979; Gierlinski et al. 1997; Poutanen, Krolik, & Ryde 1997; Dove et al. 1998).

A previous attempt to model the X/ $\gamma$  spectrum of Cygnus X-1 relied on data from Ginga and OSSE (Gierlinski et al., 1997). They showed that a thermal Comptonization model with  $kT \sim 100$  keV,  $\tau \sim 1$  plasma could fit the data, but argued that patterns found in the residual plot suggest a two component model with a hot moderate optical depth ( $\tau \sim 1-2$ ,  $kT \sim 100$  keV) plasma and an additional Wien-like component with  $kT \sim 50$  keV and  $\tau \sim 6$ . An attempt to model the broadband X-ray spectrum from 3 to 200 keV showed that the data could be fit about equally well by a variety of models - thermal Comptonization with a coronal temperature of 40 keV and an optical depth of 3.6, a different Comptonization model with a temperature of 87 keV and an optical depth of 1.6, or a cutoff power law with an index of 1.45 and a cutoff energy of 160 keV, plus an additional blackbody component, but several of the relatively good (i.e.  $\chi^2/\nu < 2$ ) fits suggested a covering fraction for Compton reflection consistent with zero (Dove et al., 1998).

What the past analyses lack and these analyses provide is full broadband coverage from 3 to 1000 keV. The combination of Ginga and OSSE leaves a gap from roughly 30 to 50 keV where the reflection component most affects the broadband spectrum while the use of RXTE alone fails to reach the energies where the spectrum cuts off most steeply at  $\sim 400$  keV. Here we present the results of joint RXTE/OSSE fits to the spectrum of Cygnus X-1 taken in December of 1998. These data present the first gap-free energy spectra of Cygnus X-1 from 3 to 1000 keV.

## 2 OBSERVATIONS

We examine data from three OSSE viewing periods where there was simultaneous RXTE data. The color changes measured in the PCA and in the ASM over the one week periods are very small (less than a few percent; see Figure 1a for the PCA colors), suggesting that the spectrum remains stable over these time periods. Also, the ASM summed band intensities (1.3-12.0 keV) show a correlation timescale of about 20 days (see Figure 1b; the 1996 data have been excluded so the measure will not be biased by the state transition that occurred then). The OSSE fluxes in the highest energy bands are weak and only detectors 3 and 4 from OSSE were turned on. Hence the full OSSE viewing periods, rather than just the strictly simultaneous data, are used as the average spectra for the analysis. The data are extracted using the standard reduction procedure from the CGRO science center.

The RXTE data are analyzed using the standard RXTE GOF criteria for spectral extraction. Data from only the top layers are used, and all five PCUs are added together. The HEXTE data are also extracted using the standard reduction criteria. The data used from each instrument is presented in Table 1.

## 3 ANALYSIS

The data are then fit with the EQPAIR model using XSPEC 11.0 (Arnaud 1996). The model allows for thermal and non-thermal Comptonization of soft photons, pair production, Compton reflection, and bremsstrahlung emission. The physics of the model are described in detail in Coppi (1998). It has previously been used to fit spectra from Cyg X-1 (Gierlinski et al. 1997; Frontera et al. 2001), GX 339-4 (Nowak, Wilms & Dove 2002) and GRS 1915+105 (Maccarone, Coppi & Taam 1999; Maccarone 2001; Zdziarski et al. 2001). One percent systematic errors are added to all channels. Many of the parameters are frozen. The inclination angle is assumed to be 55 degrees, in agreement with the most recent measurements (Sowers et al, 1998). The compactness,  $\ell_{bb}$  ( $\ell_{bb} = L_{bb}\sigma_T/m_e c^3 R_{cor}$ , where  $L_{bb}$  is the luminosity of the seed blackbody photon distribution,  $\sigma_T$  is the Thomson cross-section,  $m_e$  is the electron mass, and  $R_{cor}$  is the radius of the emission region) of the seed photon distribution is assumed to be unity. The elemental abundances are assumed to be solar. The reflector's temperature is assumed to be 100 eV. The overall normalizations of the HEXTE and OSSE components are allowed to float, but are extremely well constrained since even small deviations

(i.e.  $\sim 1\%$ ) from the best fit normalizations will produce extremely statistically significant discontinuities in the spectra. The PCA data are fit from 3 to 20 keV, the HEXTE from 17 to 190 keV and the OSSE from 100 to 1000 keV. Additional model components of neutral hydrogen column absorption and a gaussian component to fit the iron emission line are also included. Since RXTE is not sensitive to the energies where absorption by the interstellar medium is most important, the neutral hydrogen column is fixed to  $5 \times 10^{21}$  in accordance with ASCA and BeppoSax results (Gierlinski et al. 1999; Frontera et al. 2001). The iron line is restricted to fall between 6.1 and 7.0 keV in energy and to be less than 1.2 keV in width. The parameters that are allowed to vary freely are the temperature of the seed blackbody photon distribution ( $kT_{bb}$ ), the thermal electron compactness ( $\ell_{th}$ ), the reflection fraction,  $R$  and the ionization parameter  $\xi$ , as well as an overall normalization. Additionally, the HEXTE and OSSE data sets are allowed to have their normalizations float freely since the dead time correction for the HEXTE is uncertain (especially with the standard RXTE GOF distribution response matrices which we have used) as are the cross-calibrations between RXTE and OSSE. Additionally, since the data from the two satellites are not strictly simultaneous there may be some physical difference in the luminosities apart from calibration issues. Typically, the HEXTE and the OSSE are both normalized to about 70% of the PCA. We also note that these observations are typical for Cygnus X-1 as the power spectrum shows breaks at  $\sim 0.1$  Hz and  $\sim 5$  Hz, which are approximately the median values for the break frequencies (Pottschmidt et al., 2001). Since the spectral indices tend to change much less than the variability timescales (see e.g. Belloni & Hasinger 1990), and the two are well correlated, this represents strong evidence that the observations are typical.

### 3.1 Pure thermal Comptonization model fits

The results of the fitting are presented in Table 2. A typical spectral fit is plotted in Figure 2. The residuals to this fit are shown in Figure 3. Most of the parameters vary little from observation to observation, in accord with the result that the colors in the PCA bands vary little over this time span. The parameters that change the most are the iron line equivalent width, the ionization parameter for the reflection, and the and the iron line's physical width. Since these parameters are all most sensitive to the region between 6 and 8 keV (the ionization level parameter depending primarily on the energy of the iron absorption edge), where there are not sufficient independent energy bins to fit the required number of parameters, one cannot be confident that the differences are real. Furthermore, the best fit equivalent widths of the iron lines are of order 100 eV for these observations. Previous measurements of the iron line for Cygnus X-1 in the hard state from ASCA show  $\sim 20$  eV equivalent width (Ebisawa et al. 1996). RXTE fits to the Crab spectrum can suggest the presence of an iron line with an equivalent width of about 80 eV, so features this weak should not be trusted regardless of the formal statistical significance of the result. Errors in the iron line measurements can lead to significant errors in the edge position. That the line energies are found to be below 6.4 keV at a strong significance level (in disagreement with results from ASCA) also indicates that the

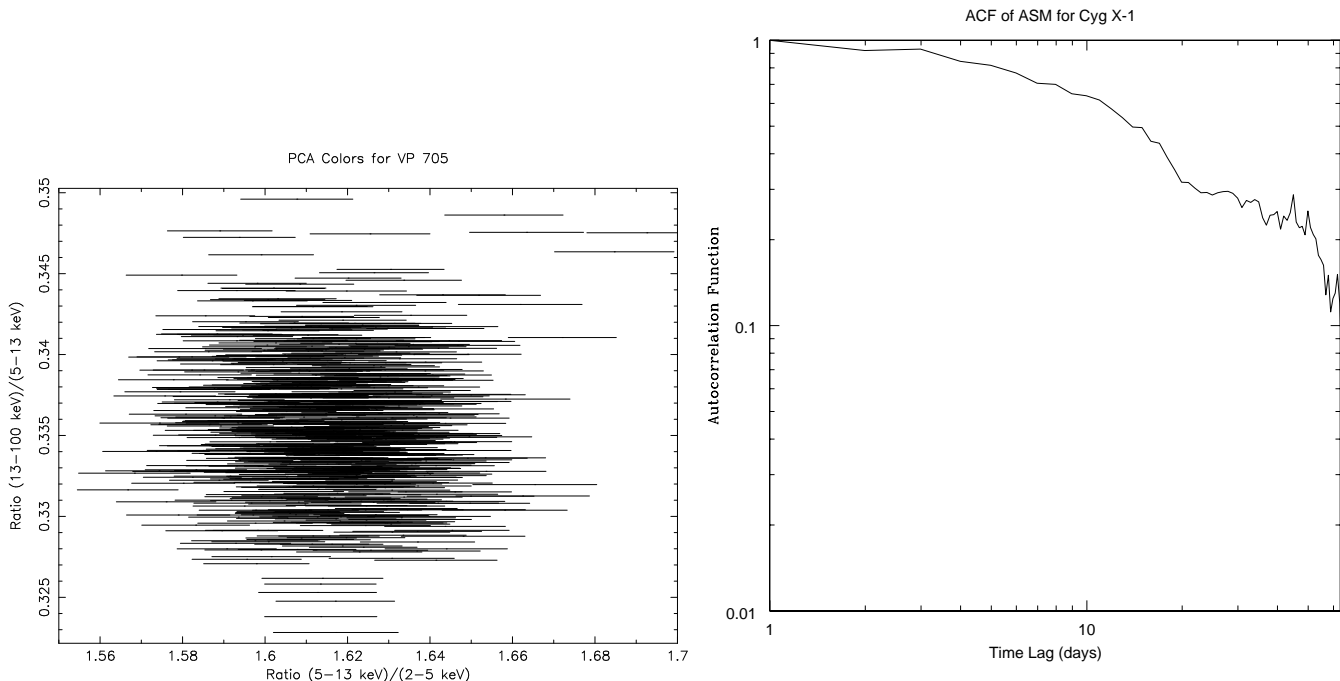


**Figure 1.** (a) The PCA colors over the first week of the observation. The colors change very little within the observations and by only a few percent from observation to observation. A few points are omitted from the plot near zero orbital phase where nH variations make a large difference in the colors and count rates (b) The autocorrelation function of the summed band (1.3-12.0 keV) ASM lightcurve.

narrow feature is more likely related to errors in the response matrix than to a real physical feature.

Other than the line parameters, a clear picture for the spectrum emerges where the disk temperature is fit to be between 150 and 250 eV, the ratio of thermal compactness to seed photon compactness is about 9, and the optical depth is about 1.3. Thus previous results that the corona of Cygnus X-1 in the hard state can be well fit as a photon-starved thermal plasma of moderate optical depth are verified. We have done several simulations and found that changes in the blackbody temperature can be measured due to changes in the curvature of the “power law” component of the spectrum at energies well in excess of the blackbody peak. For these observations, the blackbody temperatures vary very little; this model would be sensitive to variations about twice as large. Since slightly different models for the blackbody seed photon distribution can change the observed temperature and because of uncertainties in the RXTE response matrix and the lack of an RXTE response below 2 keV where the blackbody peaks, *absolute* measurements of the seed photon temperature should be treated with skepticism. Relative changes, however, can be reliably measured.

### 3.2 Hybrid Thermal/Non-thermal Comptonization model fits

Additional fits are made with the inclusion of a non-thermal component to the spectrum. That is to say, the electron distribution then consists of a Maxwellian distribution (the “thermal” Comptonization component) and a power law component (the “non-thermal” Comptonization component, which is restricted to have electron Lorentz factors from 1.3 to 1000 and has a compactness  $\ell_{nth}$  and an electron spec-

tral index of  $\Gamma$  such that  $\frac{dN}{dE} \sim E^{-\Gamma}$ ). The value of  $\Gamma$  is required to be greater than 1, the hardest electron spectrum that can be produced by standard acceleration processes. The best fit parameters are shown in Table 3. These fits are marginally better than those without the non-thermal component, with improvements in likelihood of factors of about 5 for VP 705 and VP 706 (which are best fit by a nearly purely *non-thermal* Comptonization model), and no improvement in VP 707. Since it is unlikely that a major qualitative change (i.e. whether the corona is dominated by thermal or non-thermal electrons) has occurred while the spectra look almost identical, we also attempt to fit a model to the data with a purely non-thermal electron for VP 707. We find that the data are consistent with this model as well ( $\chi^2/\nu = 1.04$ ), with  $\Gamma_{inj} = 3.3$ ,  $\ell_{nth} = 8.5$ , and the other parameters consistent with their values for both the pure thermal and the hybrid model cases.

The difficulty of distinguishing a thermal plasma from a hybrid one has been discussed previously. It has been noted that a hybrid plasma and a purely thermal plasma will produce nearly identical spectra given the same optical depth and the same mean energy shift per scattering (Zdziarski, Coppi, & Lamb 1990; Ghisellini, Haardt, & Fabian 1993). Still theoretical models do predict differences between the two plasmas above  $\sim 400$  keV (see Figure 4), since the purely thermal Comptonization models will show a nearly exponential decay, while the hybrid models will show a power law decay. Distinguishing between these two best fits would require sensitivity at the  $4 \times 10^{-6}$  photons/cm<sup>2</sup>/sec level, which is beyond the capability of the existing OSSE observations. A  $10\text{-}\sigma$  detection of this feature should be feasible with INTEGRAL in  $\sim 10^6$  seconds, and with ASTRO-E2 in about  $10^5$  seconds. Measurements from COMPTEL also

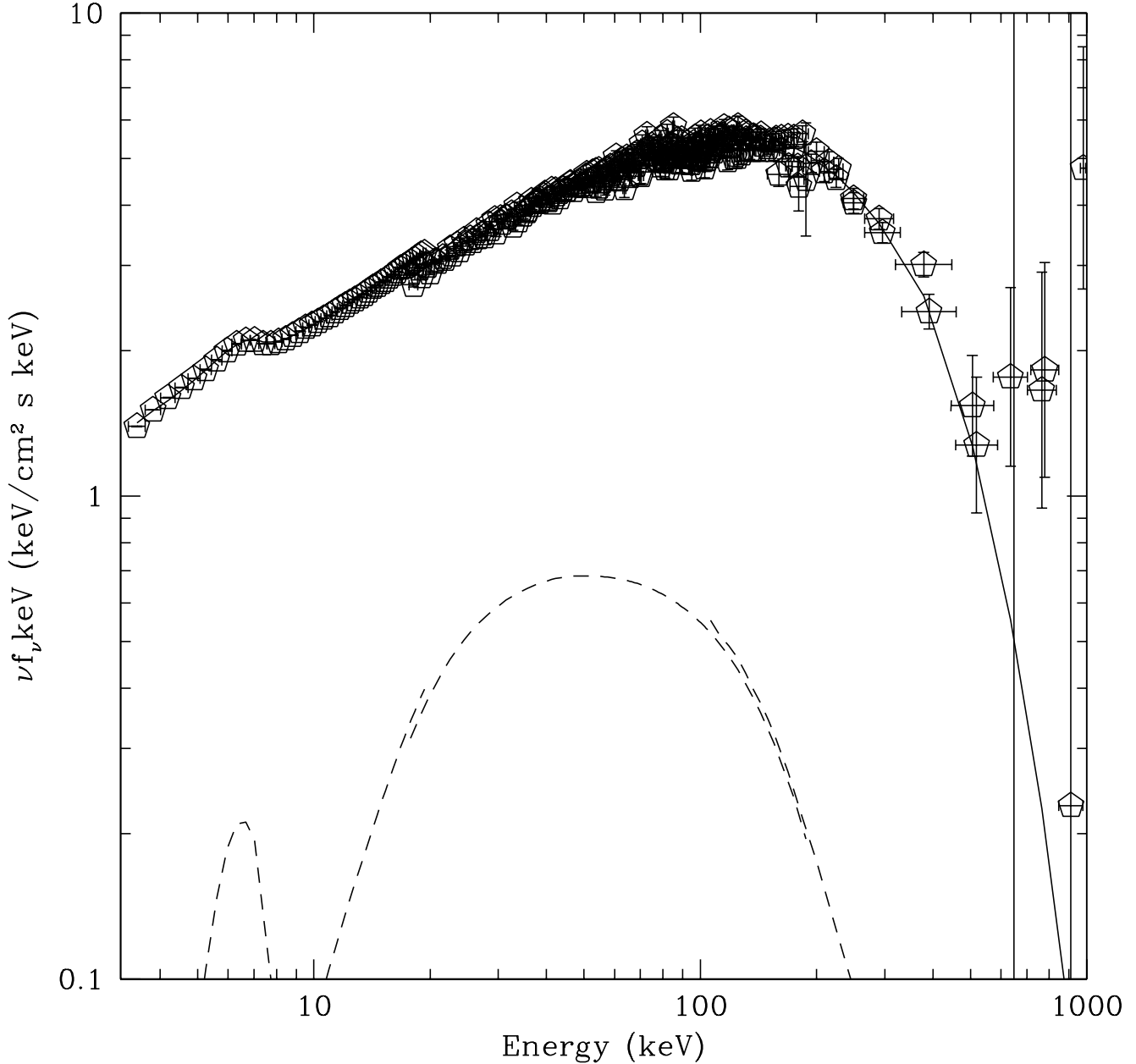


**Figure 2.** The unfolded thermal Comptonization fit to the data for OSSE viewing period 707, plotted in  $E^2 \frac{dN}{dE}$  units. The data are in open pentagons, the model fits in the solid line and the reflection component in the dashed line. The PCA component has been multiplied by 0.7 to make its relative normalization approximately the same as those for HEXTE and OSSE.

seem to suggest the presence of an extended tail to the spectrum (McConnell et al., 2000), but these observations are not taken simultaneously with X-ray detections and also require long integrations over which variability of the coronal temperature could be important.

### 3.3 The Overall Compactness and the Size of the Emission Region

We also investigate the range of overall compactnesses allowed by the data to determine whether constraints can be placed on the radius of the emission region and on the fraction of the coronal optical depth that is  $e^-/e^+$  pairs. We re-fit the model for VP 707 with a purely thermal electron distribution, while varying  $\ell_{bb}$ . We find at the 90% confidence level that the total compactness of the system cannot ex-

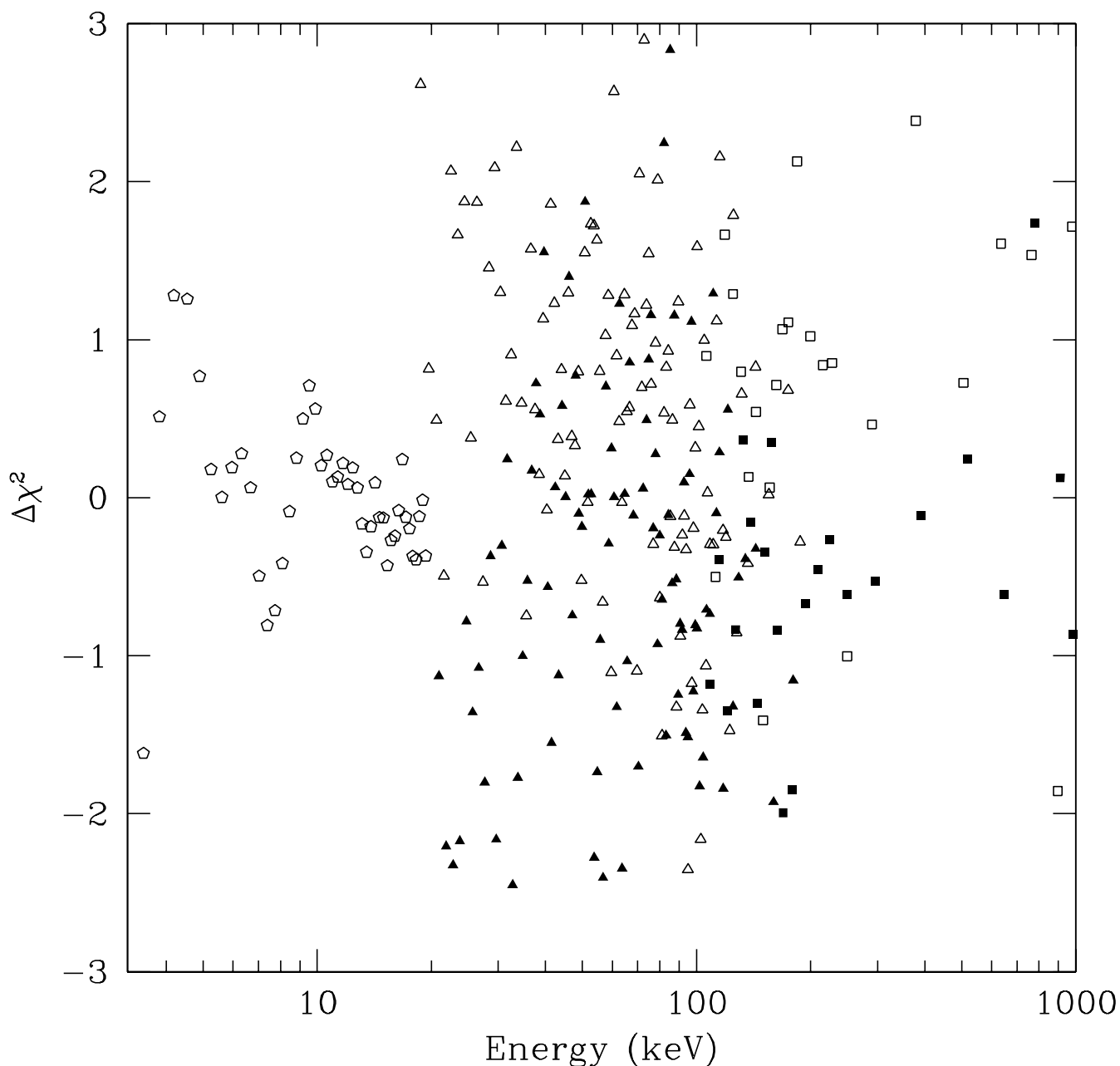


**Figure 3.** The residuals to the fit for OSSE viewing period 707, plotted as  $\Delta\chi^2$  versus energy. The PCA points are open pentagons, the HEXTE cluster 0 points are open triangles, the HEXTE cluster 1 points are filled triangles, the OSSE cluster 3 points are open squares and the OSSE cluster 4 points are filled squares.

ceed  $\sim 300$ . This constraint requires that  $R_{cor} > 3 \times 10^6$  cm, which is not a strong constraint since this value is  $\sim 1R_{SCH}$  for a  $10 M_{\odot}$  black hole. We also find that the total compactness cannot drop below  $\sim .06$  or the bremsstrahlung cooling rate will dominate the Compton cooling rate, yielding a bremsstrahlung emission spectrum which has too sharp a cutoff at high energies. This constraint requires that  $R_{cor} < 1.5 \times 10^{10}$  cm. This provides a spectral confirmation that the  $\sim$  few second hard time lags seen in variability analyses cannot be produced by light travel times in a large

corona as had been suggested previously (see e.g. Kazanas, Hua, & Titarchuk 1997) and refuted on the basis of variability measurements (Maccarone, Coppi, & Poutanen 2000).

We conduct the same analysis to find the minimum and maximum compactness for the purely non-thermal spectral fit to VP 707. The best fit is for  $\ell_{bb} = 1.5 \pm_{0.3}^{2.5}$ . The tighter bound in the lower direction is because there is some intrinsic curvature to the spectrum and some  $\gamma$ - $\gamma$  pair production is needed to reproduce this. The tighter bound in the upward direction is because the annihilation peak at 511 keV

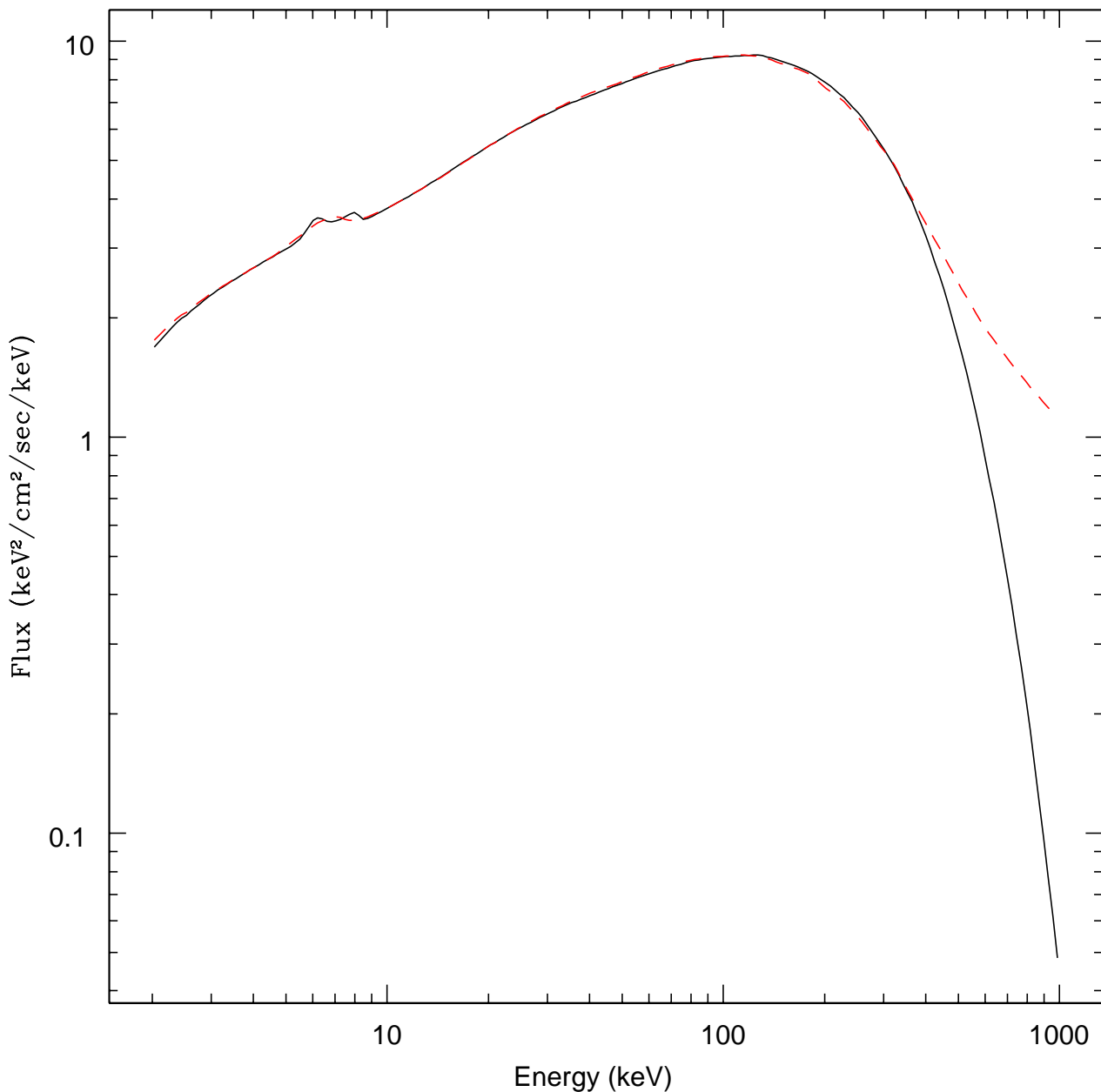


**Figure 4.** The plot of the thermal and non-thermal fits to the spectrum from VP 706, folded through an idealized response matrix. Note that the differences are only apparent above  $\sim 400$  keV.

is much sharper for non-thermal Comptonization than for thermal Comptonization (i.e. in the thermal Comptonization case, the annihilation line is reddened and broadened significantly by Compton scattering off the thermal electrons - see Coppi 1998). These constraints require a corona with a size scale between  $2 \times 10^8$  and  $7 \times 10^8$  cm. This result is not very sensitive to letting  $\gamma_{min}$  float freely, so if a purely non-thermal electron distribution can be proven to exist, fairly strong constraints can be placed on the size of the emission region. A hybrid model (rather than purely non-thermal) pro-

duces similarly tight constraints as the purely non-thermal model ( $\ell_{bb} = 2.2 \pm 1.5$ ).

### 3.4 The reflection fraction

The relatively low reflection fractions in Cyg X-1 and other X-ray binaries have been explained as coming from a geometric effect where there is a “hole” inside the inner edge of the accretion disk from which no reflection comes (Gilfanov et al., 1999), a beaming effect due to a mildly relativistic outflow from the disk (Beloborodov 1999), smearing of the

reflected component as it passes back through the corona (Petrucci et al., 2001) or an underestimate of the reflection fraction due to a highly ionized disk (Young et al. 2001). We test the last of these mechanisms on VP 707 by allowing freezing the ionization parameter at a value of  $10^5$ . We find that even for this large ionization parameter, the reflection fraction remains  $\sim 0.35$ . Furthermore, the spectral fits are substantially poorer ( $\Delta\chi^2 \sim 150$ ) than the best fits, which are obtained with low ionization parameters. We also ignore the PCA data from 5.0 to 9.5 keV and re-fit the model to ensure that the iron line and edge have no impact on the best fit parameters and find that none of the parameters change. The reason for the discrepancy between this work and that of Young et al. (2000) is likely that the reflection fraction in the ASCA/Ginga data sets they fit depends largely on the location and strengths of the iron edges since ASCA has no sensitivity above 10 keV and Ginga has none above 30 keV, while in our fits, the reflection fraction depends largely on the curvature of the spectrum in the 30-50 keV range, since there are many more bins in this region than the 6-9 keV region where the iron line and edge are found. We have also fit the data after removing the OSSE data and have found essentially the same fit as for the PCA and HEXTE data alone.

### 3.5 Robustness of the fits to changes in the frozen parameters

We investigate the robustness of the spectral fits to changes of several parameters that have been left frozen. We find that changing the seed photon distribution to a diskPN model, which gives the sum of several blackbodies as from a pseudo-Newtonian disk (Gierlinski et al., 1999), rather than a pure blackbody yields a slightly higher optical depth ( $\tau \sim 1.4$ ) and a higher thermal compactness ( $\ell_{th} \sim 12$ ) without making any qualitative changes to the spectrum or the overall goodness of fit. We find that for the nonthermal model,  $\gamma_{min}$  can be increased to  $\sim 3$  without affecting the quality of the fit. For such high values of  $\gamma_{min}$ , the electron injection distribution approaches a  $\delta$ -function, so these fits are probably unphysical, and it is unlikely that the non-thermal electron distribution is cut off much below 200 keV.

## 4 CONCLUSIONS

We find that the 3-1000 keV spectrum of Cygnus X-1 in the hard state can be well fit by a purely thermal Comptonization model, but that a substantial (and perhaps dominant) non-thermal component cannot be ruled out. For a thermal model, we find typical temperatures of the corona to be  $\sim 90$  keV, with optical depths of  $\sim 1.3$ , and that for two of the observations, the data can be modelled slightly better with a purely nonthermal electron distribution. We find no evidence for the existence of an additional optically thick component in the spectrum. We find that the data are insufficient to differentiate between a pair-dominated corona and an electron/ion dominated corona. We find that the reflection fractions are low (i.e.  $R/2\pi < 1$ ) because there is relatively little spectral curvature in the 30-50 keV range and not due to a ionization effects in the disk. Future observations with instruments such as INTEGRAL and ASTRO-

E2 should prove capable of breaking the degeneracy between the thermal and non-thermal electron distributions by measuring the emission at several MeV more accurately than current data sets which have provided simultaneous X-ray measurements.

## 5 ACKNOWLEDGMENTS

We wish to thank Jörn Wilms and Mike Nowak for scripts that facilitated finding the errors in the spectral fits.

## REFERENCES

- Arnaud, K.A., 1996, in ASP Conf. Series 101, *Astronomical Data Analysis Software and Systems V* (eds: G.H. Jacoby & J. Barnes), ASP: San Francisco
- Belloni, T. & Hasinger, G., 1990, *A&A*, 227, L33
- Beloborodov, A.M., 1999, *ApJL*, 510, 123
- Coppi, P.S., 1998, “The Physics of Hybrid Thermal/Non-Thermal Plasmas” in *High Energy Processes in Accreting Black Holes*, eds. J. Poutanen and R. Svensson, ASP Conf. Series, Vol. 161, p. 375 (astro-ph/9903158)
- Dolan, J.F., 1992, *ApJ*, 384, 249
- Dove, J.B., Wilms, J., Nowak, M.A., Vaughan, B.A., & Begelman, M.C., 1998, *MNRAS*, 298, 729
- Ebisawa, K., Ueda, Y., Inoue, H., Tanaka, Y., & White, N.E., 1996, *ApJ*, 467, 419
- Frontera, F., Palazzi, E., Zdziarski, A.A., Haardt, F., Perola, G.C., Chiapetti, L., Cusumano, G., Dal Fiume, D., Del Sordo, S., Orlandini, M., Parmar, A.N., Piro, L., Santangelo, A., Segreto, A., Treves, A., & Trifoglio, M., 2001, *ApJ*, 546, 1027
- Ghisellini, G., Haardt, F., & Fabian, A.C., 1993, *MNRAS*, 263, L9
- Gierlinski, M., Zdziarski, A.A., Done, C., Johnson, W.N., Ebisawa, K., Ueda, Y., Haardt, F., & Philips, B., 1997, *MNRAS*, 288, 958
- Gierlinski, M., Zdziarski, A.A., Poutanen, J., Coppi, P.S., Ebisawa, K., & Johnson, W.N., 1999, *MNRAS*, 309, 496
- Gies, D.R., & Bolton, C.T., 1986, *ApJ*, 304, 371
- Gilfanov, M., Churazov, E., & Revnivtsev, M., 1999, *A&A*, 352, 182
- Kazanas, D., Hua, X.-M., & Titarchuk, L., 1997, *ApJ*, 480, 735
- Maccarone, T.J., 2001, Ph.D. Thesis, Yale University
- Maccarone, T.J., Coppi, P.S., & Poutanen, J., 2000, *ApJL*, 537, 107L
- Maccarone, T.J., Coppi, P.S. & Taam, R.E., 1999, *BAAS*, 195, 3703
- McConnell, M.L., Ryan, J.M., Collmar, W., Schönfelder, V., Steinle, H., Strong, A.W., Bloemen, H., Hermsen, W., Kuiper, L., Bennett, K., Philips, B.F., & Ling, J.C., 2000, *ApJ*, 543, 928
- Nowak, M.A., Wilms, J. & Dove, J.B., 2002, *MNRAS*, in press (astro-ph/0201383)
- Petrucci, P.O., Merloni, A., Fabian, A.C., Haardt, F. & Gallo, E., 2001, astro-ph/0108432
- Pottschmidt, K., Wilms, J., Nowak, M.A., Pooley, G.G., Gleissner, T., Heindl, W., Smith, D.M., & Staubert, R., 2001, astro-ph/0202258
- Poutanen, J., Krolik, J.H., & Ryde, F., 1997, *MNRAS*, 292, L21
- Sowers, J.W., Gies, D.R., Bagnulo, W.G., Shafter, W., Wiemker, R., & Wiggs, M.S., 1988, *ApJ*, 506, 424
- Sunyaev, R., & Trümper, J., 1979, *Nature*, 279, 506
- Young, A.J., Fabian, A.C., Ross, R.R., & Tanaka, Y., 2001, *MNRAS*, 325, 1045
- Zdziarski, A.A., Coppi, P.S., & Lamb, D.Q., 1990, *ApJ*, 357, 149

Observations Analyzed for This Work		
ObsID	Start Time	Stop Time
30158-01-01-00	10/12/97 07:07:53	10/12/97 08:30:14
30158-01-02-00	11/12/97 07:06:14	11/12/97 08:45:14
30158-01-03-00	14/12/97 08:48:14	14/12/97 10:20:14
30158-01-04-00	15/12/97 03:49:42	15/12/97 05:26:14
30158-01-05-00	15/12/97 05:26:14	15/12/97 07:09:14
30158-01-06-00	17/12/97 00:39:55	17/12/97 02:05:14
30158-01-07-00	20/12/97 07:11:18	20/12/97 08:29:14
30158-01-08-00	21/12/97 05:28:14	21/12/97 07:05:14
30158-01-09-00	24/12/97 23:03:14	24/12/97 00:39:14
30158-01-10-00	25/12/97 00:39:14	25/12/97 01:45:14
30158-01-11-00	30/12/97 02:18:03	30/12/97 03:52:14
30158-01-12-00	30/12/97 03:52:14	30/12/97 05:30:14
Viewing Period	Start Time	Stop Time
705	1997-12-09 17:44:24	1997-12-16 14:08:23
706	1997-12-16 16:54:51	1997-12-23 13:27:23
707	1997-12-23 16:18:54	1997-12-30 14:15:46

**Table 1.** The RXTE and OSSE observation times. VP 705 in OSSE coincides with RXTE observations 30158-01-01-00 through 30158-01-05-00, VP 706 coincides with 30158-01-06-00 through 30158-01-08-00 and VP 707 coincides with 30158-01-09-00 through 30158-01-12-00.

VP	$kT_{bb}$	$\ell_{th}$	$\tau$	Best Fit Parameters for the Thermal Model							EqW	$\chi^2/\nu$
				$R$	$\xi$	$F$	LE	LW	LN			
705	$151^{+29}_{-22}$	$9.15^{+55}_{-65}$	$1.26^{+02}_{-03}$	$.23^{+01}_{-02}$	$590^{+170}_{-170}$	$3.5 \times 10^{37}$	$6.1^{+.2}_{-**}$	$.29^{+.29}_{-.27}$	$.0054^{+.0021}_{-.0021}$	60	1.17	
706	$169^{+15}_{-35}$	$9.12^{+52}_{-30}$	$1.31^{+02}_{-05}$	$.23^{+01}_{-01}$	$486^{+120}_{-70}$	$3.7 \times 10^{37}$	$6.1^{+.1}_{-**}$	$.34^{+.32}_{-.34}$	$.0063^{+.0011}_{-.0014}$	70	1.13	
707	$233^{+18}_{-25}$	$8.49^{+51}_{-20}$	$1.30^{+02}_{-05}$	$.227^{+.016}_{-.010}$	$0.22^{+3.0}_{-.22}$	$3.3 \times 10^{37}$	$6.1^{+.1}_{-**}$	$.97^{+.15}_{-.22}$	$.015^{+.03}_{-.03}$	200	1.03	

**Table 2.** The best fit parameter values for the pure thermal Comptonization model. The error bars represent 90% confidence levels, while the double asterisks indicate parameters for which the 90% confidence level is outside the range allowed *a priori*.

Zdziarski, A.A., Grove, J.E., Poutanen, J., Rao, A.R. & Vadawale, S.V., 2001, ApJL, 554, 45



## Best Fit Parameters for the Hybrid Model

VP	$kT_{bb}$	$\ell_{th}$	$\ell_{nth}$	$\Gamma$	$\tau$	$R$	$\xi$	LE	LW	LN	EqW	$\chi^2/\nu$
705	$192^{+28}_{-21}$	$0.18^{+0.29}_{-0.18}$	$8.55^{+1.45}_{-1.55}$	$3.0^{+0.1}_{-0.10}$	$1.342^{+0.005}_{-0.015}$	$.233^{+0.003}_{-0.020}$	$410^{+190}_{-130}$	$6.1^{+0.2}_{-0.22}$	$.28^{+0.31}_{-0.28}$	$.0054^{+0.0030}_{-0.0014}$	60	1.12
706	$197^{+6}_{-10}$	$0.04^{+0.14}_{-0.04}$	$8.73^{+0.16}_{-0.13}$	$3.14^{+0.14}_{-0.15}$	$1.367^{+0.005}_{-0.005}$	$.236^{+0.009}_{-0.026}$	$16^{+200}_{-2}$	$6.1^{+0.1}_{-0.22}$	$1.0^{+0.1}_{-0.1}$	$.019^{+0.003}_{-0.003}$	220	1.07
707	$258^{+28}_{-34}$	$6.38^{+1.63}_{-3.38}$	$2.36^{+0.99}_{-0.99}$	$2.1^{+0.5}_{-0.5}$	$1.31^{+0.02}_{-0.06}$	$.237^{+0.016}_{-0.027}$	$5^{+470}_{-5}$	$6.1^{+0.2}_{-0.22}$	$.91^{+0.23}_{-0.35}$	$.013^{+0.004}_{-0.003}$	180	1.04

**Table 3.** The best fit parameter values for the pure thermal Comptonization model. The error bars represent 90% confidence levels, while the double asterisks indicate parameters for which the 90% confidence level is outside the range allowed *a priori*.